AVO modeling of monochromatic spherical waves: comparison to band-limited waves

Charles P. Ursenbach and Arnim B. Haase

ABSTRACT

Monochromatic and band-limited spherical waves have differing reflection coefficient curves. To make a comparison of these two paradigms, a new expression for the monochromatic reflectivity is given in terms of a weighting function. The weighting function approach, developed previously for a specific class of band-limited spherical waves (Rayleigh wavelets), shows explicitly how different plane waves contribute to the spherical-wave reflection coefficient. Direct comparison shows that monochromatic waves have oscillatory, non-decaying weighting functions, and thus sample a wide range of plane waves. This contrasts with typical Rayleigh wavelets which have well-localized weighting functions. These two behaviors lead to reflection coefficient curves which are respectively oscillatory and monotonic after the critical angle. A bridge between these two behaviors is constructed by considering unusually narrow Rayleigh wavelets. These show intermediate properties. The benefits of this study are 1) a simple and convenient method for calculating monochromatic spherical-wave reflection coefficients, and 2) a clearer understanding of how spherical-wave reflection coefficients are created from constituent plane-waves.

INTRODUCTION

Historically, the most common approach for describing reflectivity of spherical waves in seismic exploration has been through constructing the reflection coefficients for a monochromatic source. This approach was due to Lamb (1904) and Sommerfeld (1909) and is described in Aki and Richards (1980). It has been employed for instance by Krail and Brysk (1983) and MacDonald et al. (1987). Carrying out such calculations for multiple frequencies allows one to obtain the reflection coefficient for a bandlimited wavelet via an inverse Fourier transform.

Cagnaird (1939) presented an alternate approach in which an expression is given for the reflection coefficient of an impulsive wave. This has been further discussed in exploration seismology literature by Bortfeld (1962), Tygel and Hubral (1984) and Hubral and Tygel (1985). Again, a band-limited wavelet result can be obtained from this result, in this case by convolution. Thus both the monochromatic and impulsive reflection coefficients involve numerous numerical integrals to obtain band-limited reflection coefficients.

Haase has in recent years developed a flexible scheme for the calculation of bandlimited reflectivities from several monochromatic calculations (e.g., Haase (2004)). An example of the spherical-wave reflection coefficient curve for an Ormsby wavelet is given in Figure 1. There is good agreement with the plane-wave result at low and high angles, but not near the critical point of this Class 1 model. One other prominent feature of this result is the oscillatory decay back to the plane-wave result after the critical angle. Haase has also calculated reflection coefficient curves for monochromatic spherical

waves. A number of these are shown in Figure 2. Even greater oscillations are present here that apparently undergo partial cancellation to produce the band-limited Ormsby result.
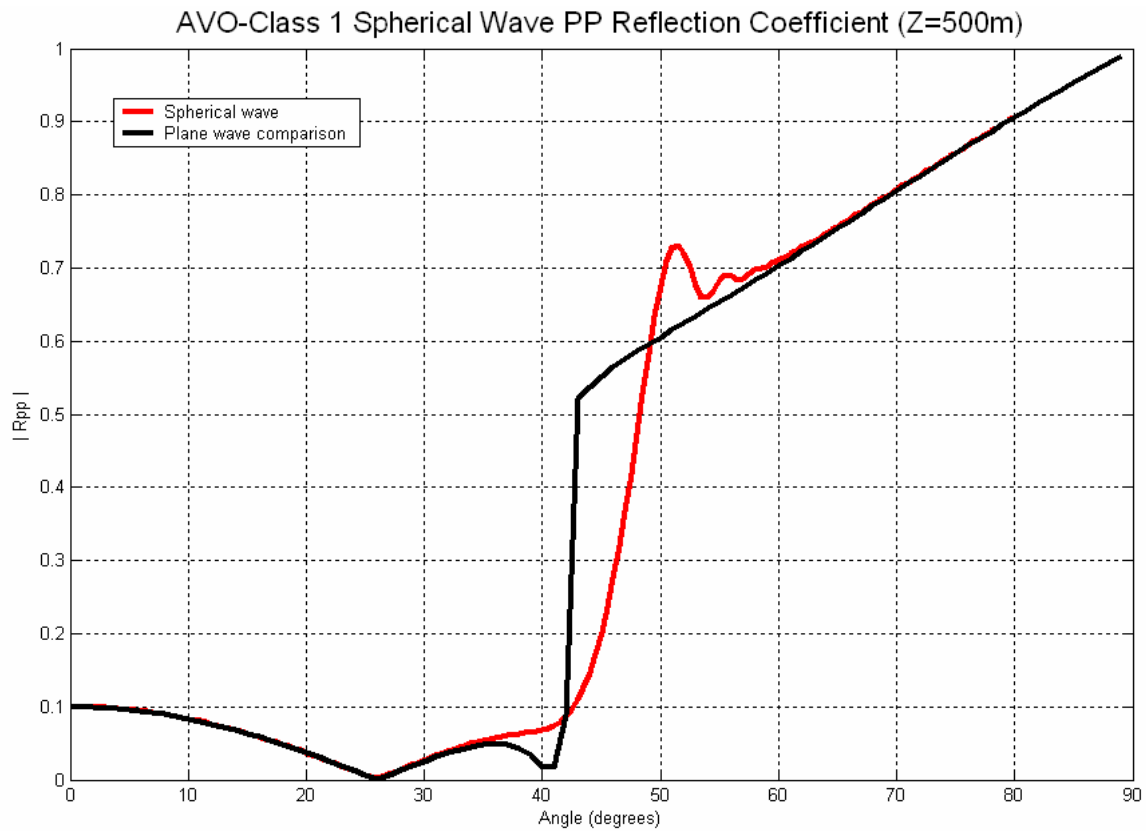

FIG. 1: Comparison of plane-wave and spherical-wave reflection coefficient curves. The two differ near the critical angle (~43°). The spherical-wave curve also becomes oscillatory above the critical angle.

AVO-Class 1 Spherical Wave PP Reflection Coefficient as Function of Frequency (Z=500m)
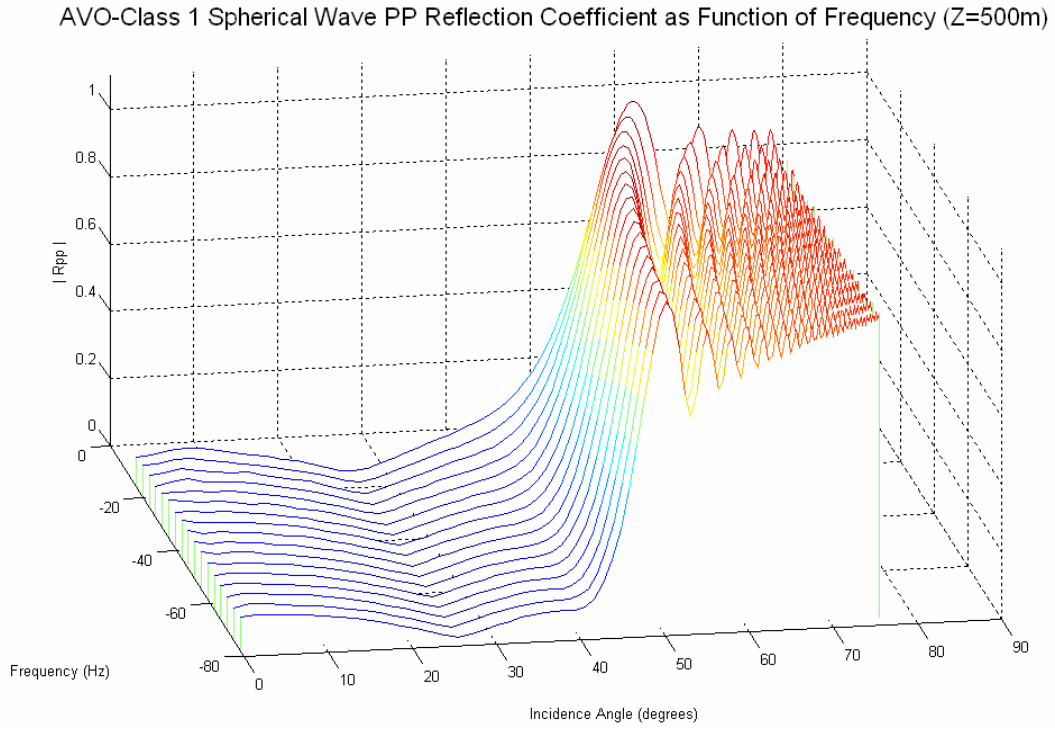

FIG. 2: Individual frequency-dependent curves that are combined to produce the spherical-wave reflection coefficient curve of Figure 1. Each line represents the spherical-wave reflection coefficient curve for a monochromatic spherical wave.

We have previously presented a direct approach to bandlimited reflection coefficients (Ursenbach and Haase, 2004). Formally this begins from the monochromatic expression, but introduces a specific wavelet, the Rayleigh wavelet (Hubral and Tygel, 1989), at the beginning of the procedure. This wavelet allows the inverse Fourier transform to be carried out analytically, before any other steps. Only one numerical integral then must be carried out to obtain the reflection coefficient for a given geometry. The final result is expressed as

$$R_{\mathrm{PP}}^{\mathrm{spherical}}(\theta_i) = \int_{\Gamma} W_n(S_0, \theta, \theta_i) R_{\mathrm{PP}}(\theta) \, d(\cos\theta), \tag{1}$$

where θ_i is the angle of incidence, θ is an integration parameter, Γ is an integration path in the complex plane, $S_0 \equiv \alpha_1/(R\omega_0)$, ω_0 is the dominant frequency of the Rayleigh wavelet, and W_n is a normalized weighting function, with n a parameter of the Rayleigh wavelet. For Rayleigh wavelets, W_n is an analytic function which can be readily programmed.

In addition to providing a speedy approach to calculating spherical-wave reflection coefficients, the Rayleigh wavelet approach of equation 1 also provides useful insight into the relationship between plane-wave and spherical-wave reflectivities. The W_n kernel is largest when θ and θ_i are similar, and decays rapidly when $|\theta-\theta_i|$ is large. Thus the spherical-wave reflection coefficient receives contributions primarily from plane-

wave coefficients near the angle of incidence. Indeed, as $S_0 \to 0$, the spherical-wave coefficient approaches the plane-wave Zoeppritz result (Ursenbach and Haase, 2004).

Because the monochromatic reflection coefficients have been considered in previous studies (Krail and Brysk, 1983; Macdonald et al., 1987), it is of interest to develop a similar understanding of how plane-wave coefficients contribute in this case. This is the subject of the present investigation.

To approach this problem we first derive an expression for the monochromatic spherical-wave reflection coefficient which is similar in form to equation 1. We may then compare monochromatic reflection coefficients to bandlimited reflection coefficients, and monochromatic weighting functions to bandlimited weighting functions. We will demonstrate that the two cases differ significantly, but that the bandlimited results approach the monochromatic results for increasingly narrow bands.

THEORY

Analogous to equation 6.30 of Aki and Richards (1980), the monochromatic potential for a reflected spherical wave may be written as

$$\phi(\omega) = Ai\omega \exp(-i\omega t) \int_0^\infty \frac{p}{\xi} R_{\mathrm{PP}}(p) J_0(\omega p r) \exp[i\omega\xi(z+h)] \, dp \qquad (2)$$

where ϕ is the spectrum of the displacement potential, ω is the frequency, A is an arbitrary scale factor, t is the time, p and ξ are horizontal and vertical slownesses, R_{PP} is the plane-wave reflection coefficient, J_0 is a zeroth-order Bessel function, r is the source-receiver offset, and z and h are the vertical distances from the interface to the receiver and source.

To obtain the displacement spectrum we must take the gradient of the potential. In particular we are interested in the component of the displacement parallel to the ray vector at the receiver, $(\sin\theta_i, 0, \cos\theta_i)$, where θ_i is the angle of incidence. We denote this displacement component as

$$u_{\parallel}(\omega) = Ai\omega \exp(-i\omega t) \int_0^\infty \frac{p}{\xi} R_{\mathrm{PP}}(p) \left[-\omega p J_1(\omega p r)\sin\theta_i + i\omega\xi J_0(\omega p r)\cos\theta_i \right] \exp[i\omega\xi(z+h)] \, dp$$

$$(3)$$

To obtain a reflection coefficient which can be compared to the plane-wave Zoeppritz coefficients, we divide this result by the displacement spectrum obtained using $R_{PP} = 1$. In this case the potential simplifies to

$$\phi^{R_{Pp}=1}(\omega) = \frac{A}{R}\exp\left[-i\omega\left(t - \frac{R}{\alpha_1}\right)\right] \qquad (4)$$

where R is the length of the raypath from source to receiver $(=\sqrt{r^2 + 4z^2})$, and α_1 is the P-wave velocity of the overburden $(=1/\sqrt{p^2 + \xi^2})$. The parallel component of the gradient in this case is just equal to the partial derivative with respect to R:

$$u_\parallel^{R_{Pp}=1}(\omega) = A\left(-\frac{1}{R^2} + \frac{i\omega}{R\alpha_1}\right)\exp\left[-i\omega\left(t - \frac{R}{\alpha_1}\right)\right]. \qquad (5)$$

The normalized monochromatic reflection coefficient is then

$$R_{PP}^{\text{spherical}}(\theta_i) = \frac{u(\omega)}{u^{R_{Pp}=1}(\omega)}$$

$$= \frac{i\omega^2\int_0^\infty \frac{p}{\xi}R_{PP}(p)\left[-pJ_1(\omega pr)\sin\theta_i + i\xi J_0(\omega pr)\cos\theta_i\right]\exp[i\omega\xi(z+h)]\,dp}{\left(-\frac{1}{R^2} + \frac{i\omega}{R\alpha_1}\right)\exp\left[i\frac{\omega R}{\alpha_1}\right]} \qquad (6)$$

We can perform a change of variables for the integration and define $\sin\theta \equiv p\,\alpha_1$ and $\cos\theta \equiv \xi\alpha_1$. Then $(p/\xi)dp = -d(\cos\theta)/\alpha_1$, and the integration path becomes complex. If we set $h = z$, and note that $z = (R/2)\cos\theta_i$ and $r = R\sin\theta_i$, then this can be written as

$$R_{PP}^{\text{spherical}}(\theta_i) =$$

$$\int_\Gamma R_{PP}\frac{\left[-J_1\left(\frac{R\omega}{\alpha_1}\sin\theta\sin\theta_i\right)\sin\theta\sin\theta_i + iJ_0\left(\frac{R\omega}{\alpha_1}\sin\theta\sin\theta_i\right)\cos\theta\cos\theta_i\right]}{-i\left(\frac{\alpha_1}{R\omega}\right)^2\left(1 + i\frac{\omega R}{\alpha_1}\right)\exp\left[i\frac{\omega R}{\alpha_1}(1 - \cos\theta\cos\theta_i)\right]}d(\cos\theta) \quad (7)$$

$$= \int_\Gamma R_{PP}\frac{\left[-J_1(\sin\theta\sin\theta_i/S)\sin\theta\sin\theta_i + iJ_0(\sin\theta\sin\theta_i/S)\cos\theta\cos\theta_i\right]}{S(1 - iS)\exp\left[i(1 - \cos\theta\cos\theta_i)/S\right]}d(\cos\theta)$$

While this may appear more complicated than equation 6, note that the integrand now depends upon only three variables, θ, θ_i, and S, where R, ω and α_1 appear only in the combination $S = \alpha_1/(R\omega)$, a quantity which provides a measure of the importance of curvature and spherical effects. We note that this is now of the form

$$R_{\mathrm{PP}}^{\mathrm{spherical}}(\theta_i) = \int_{\Gamma} W(S,\theta,\theta_i)R_{\mathrm{PP}}(\theta)\,d(\cos\theta), \qquad (8)$$

with

$$W(S,\theta,\theta_i;\mathrm{wavelet}) = \frac{\left[-J_1(\sin\theta\sin\theta_i/S)\sin\theta\sin\theta_i + iJ_0(\sin\theta\sin\theta_i/S)\cos\theta\cos\theta_i\right]}{S(1-iS)\exp\left[i(1-\cos\theta\cos\theta_i)/S\right]}. \qquad (9)$$

We have thus derived an equation of the form of equation 1, and can compare reflection coefficients and weighting functions between monochromatic waves and band-limited waves.

RESULTS

We consider a Class I AVO system defined in Table 1. We have employed this model previously (Ursenbach and Haase, 2004). The plane-wave reflection coefficients for this model are given by the solid lines in Figure 1. These coefficients are also present in the integrand of equations 1 and 8. To calculate W we also require a value of S. We assume that the frequency of the monochromatic wave is $100/\pi$ Hz, and that the depth of the interface is 500 m. From Table 1 $\alpha_1 = 2000$ m/s, so $S = .01\cos\theta_i$. Equations 8 and 9 may then be solved and the result is shown by the dashed line in Figure 3. We see that the plane-wave and spherical-wave results are very similar at low angles, they differ considerably near the critical angle, and then begin to approach each other more as the angle of incidence approaches 90°.

Table 1. Two-layer, elastic interface model employed in calculations.

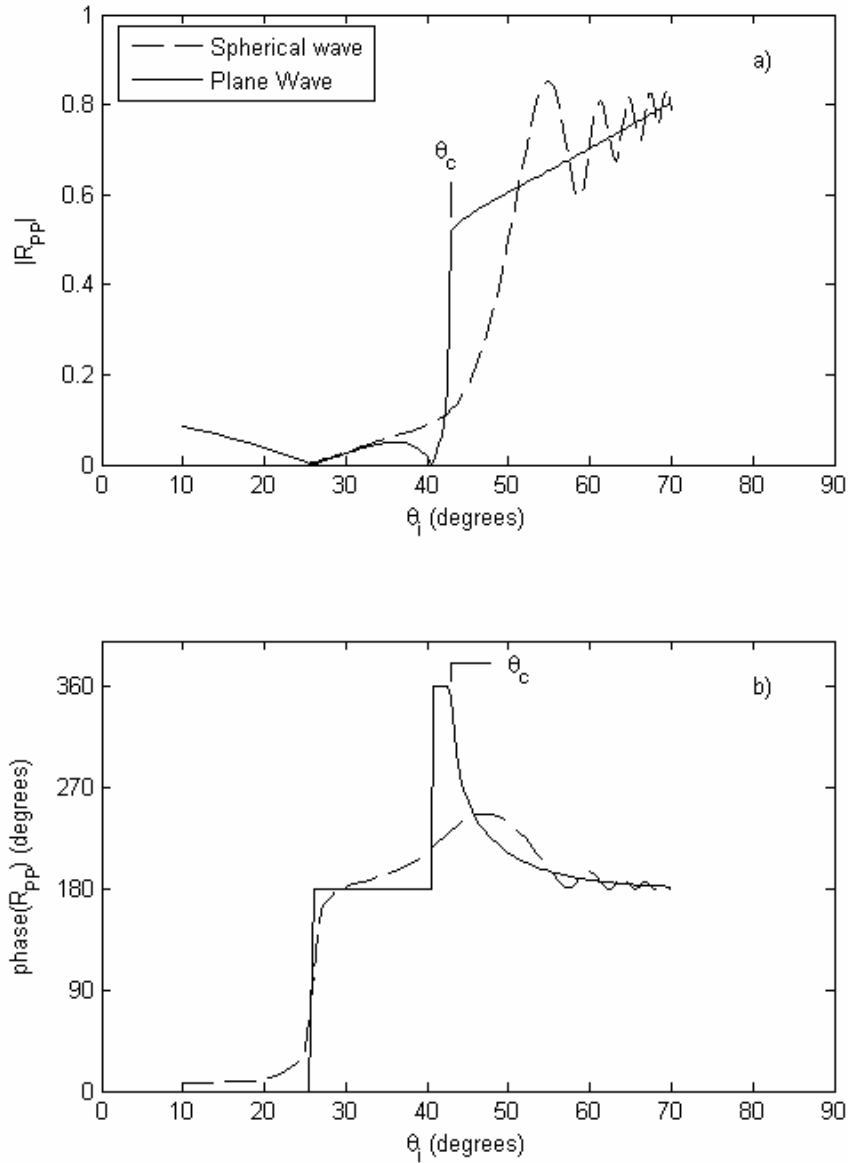|	Density (kg/m³)	P-wave velocity (m/s)	S-wave velocity (m/s)
Layer 1	2400	2000	879.88
Layer 2	2000	2933.33	1882.29

FIG. 3: Comparison of plane-wave (solid) and monochromatic spherical-wave (dashed) reflection coefficients for a Class I system. The magnitude is shown in a) and the phase in b). The spherical-wave response is strongly oscillatory past the critical angle.

Figure 3 is consistent with the behavior observed in Figure 2, and is reminiscent of the Ormsby wavelet result in Figure 2. Rayleigh wavelet reflection coefficients on the other hand approach the plane-wave result much more smoothly after the critical angle. To understand these differences we consider the weighting functions that give rise to the above reflection coefficients. In Figure 4 we plot $W(S = .02 \cos(40°), \theta, \theta_i=40°)$ from

equation 9 against θ. Also displayed is $W_4(S_0, \theta, \theta_i)$ from equation 1, with $n = 4$ and $S_0 = .02 \cos(40°)$.

In Figure 4 the most striking observation is that the two functions are most similar near the angle of incidence (40°) but bear little similarity to each other outside of that region. Away from the critical angle the bandlimited W decays quickly to zero, while the monochromatic W oscillates strongly about zero. Both of these behaviors have the effect of emphasizing plane-wave contributions near the angle of incidence. Outside the critical region the integrand of equation 1 vanishes, while the integrand of equation 9 gives rise to cancellation.
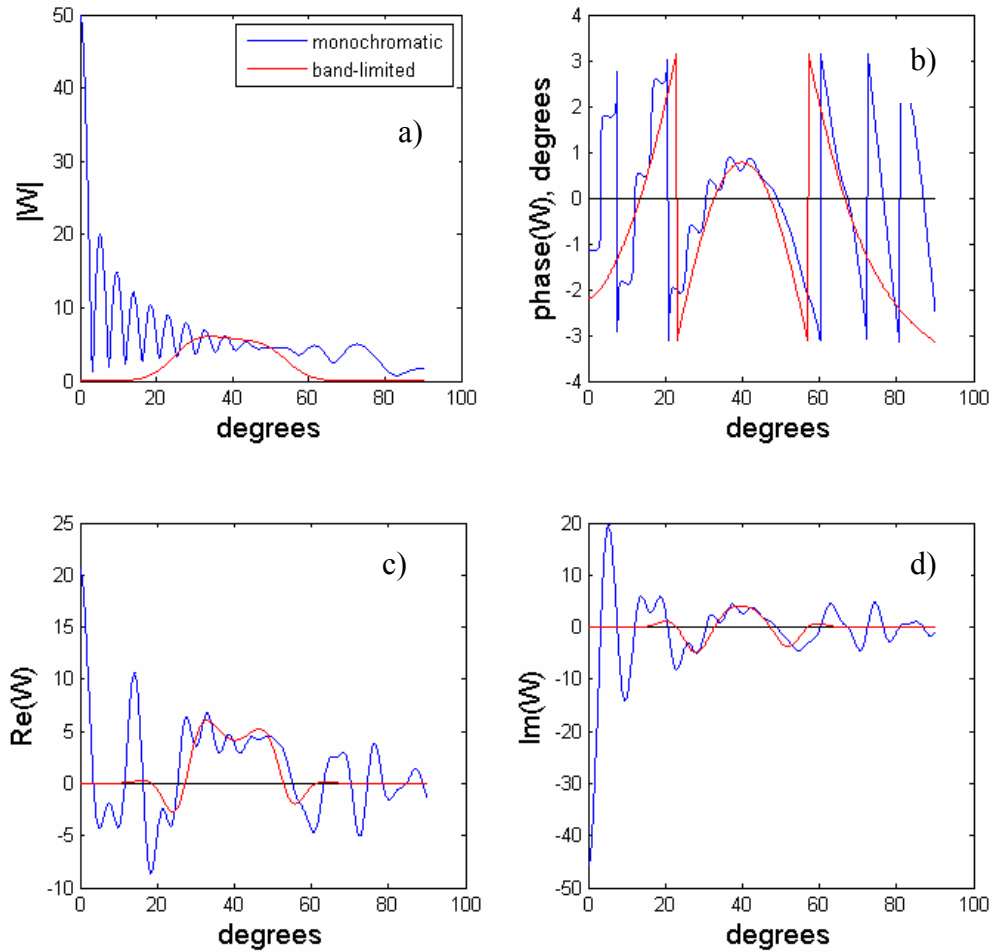

FIG. 4: Comparison of weighting functions for monochromatic and band-limited cases. The functions were obtained with similar sphericity parameters ($S = S_0$) and identical angles of incidence (40º). The greatest similarity between the functions occurs in the region of the critical angle.

We show next that it is also possible to construct a bridge between these two types of behavior. Some recent refinements of the Rayleigh wave theory (Ursenbach et al., 2006a)

have made it practical to carry out reflection coefficient calculations for large values of *n*. In Figure 5 we show three wavelet spectra having the same value of f_0 as before, but with values of *n* equal to 5 15, and 50. As *n* increases, the wavelet approaches a spike centered at f_0, and should therefore approach monochromatic behavior. Such a progression could then form a bridge between the two wavelets represented in Figure 4.
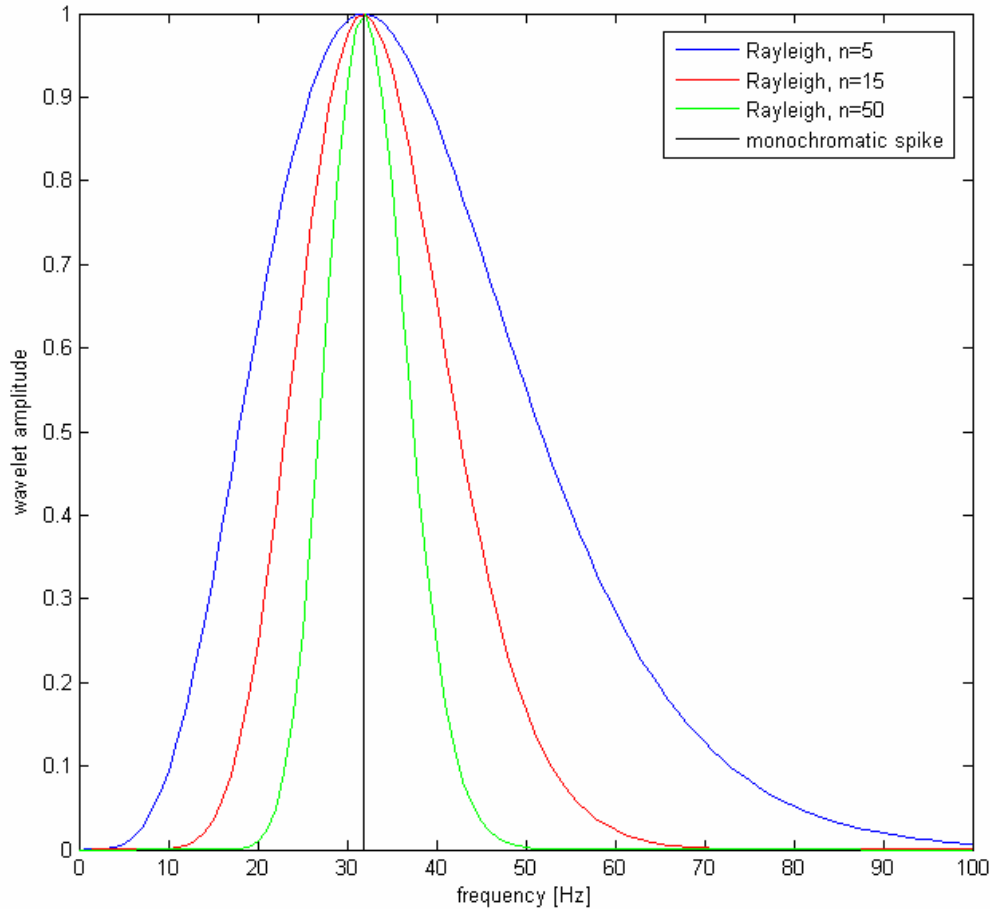

FIG. 5: The spectra of three Rayleigh wavelets, each centered at ~31.8 Hz. As *n* increases, the spectrum becomes increasingly spike-like, so that its associated reflectivity behavior should approach that of a monochromatic wavelet.

First we consider the weighting function behavior. Figure 6 displays weighting functions for the three Rayleigh wavelets and the monochromatic wavelet. The *n* = 15 and *n* = 50 wavelets do indeed form intermediates. They decay away from $\theta = \theta_i$, as does the *n* = 5 wavelet, but their decay is slower and more oscillatory, approaching the behavior of the monochromatic weighting function.
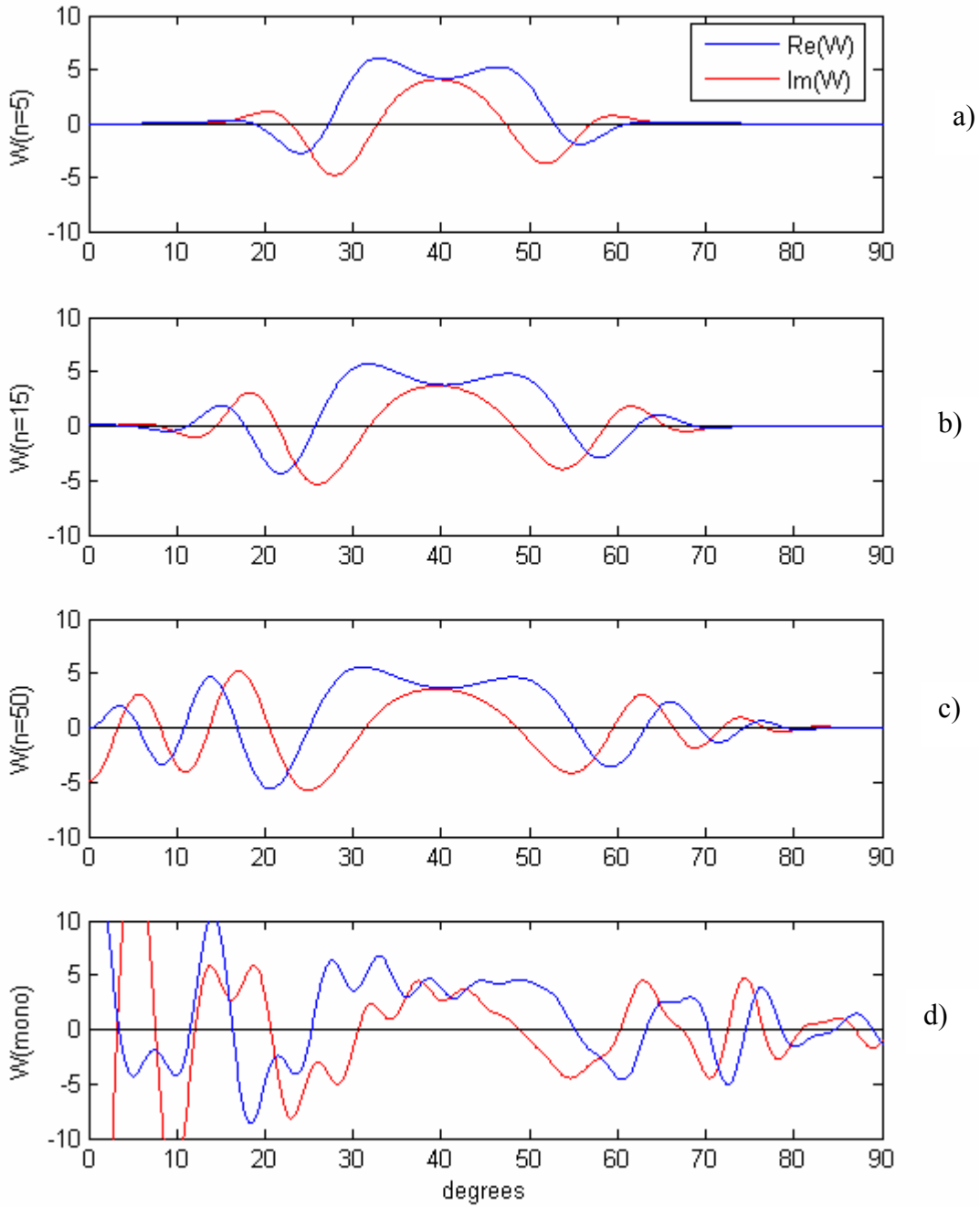
FIG. 6: The weighting functions defined at $\theta_i = 40°$ for the three wavelets in Figure 3. Note that the tails of the Rayleigh wavelet weighting functions [a)-c)] become increasingly oscillatory as *n* grows, thus approaching the appearance of the monochromatic wavelet weighting function in d)

Finally we compare the reflection coefficients calculated from such weighting functions. Figure 7 shows the four corresponding curves together. Again we see intermediate behavior for the larger *n* values. The post-critical oscillations are present, but do not persist to as high an angle as for the monochromatic case. This suggests that the post-critical oscillations are a result of oscillatory tails in the weighting functions. Thus framing calculations in terms of weighting functions, as in equations 1 and 9 provides insight into spherical-wave calculations for different types of wavelets.
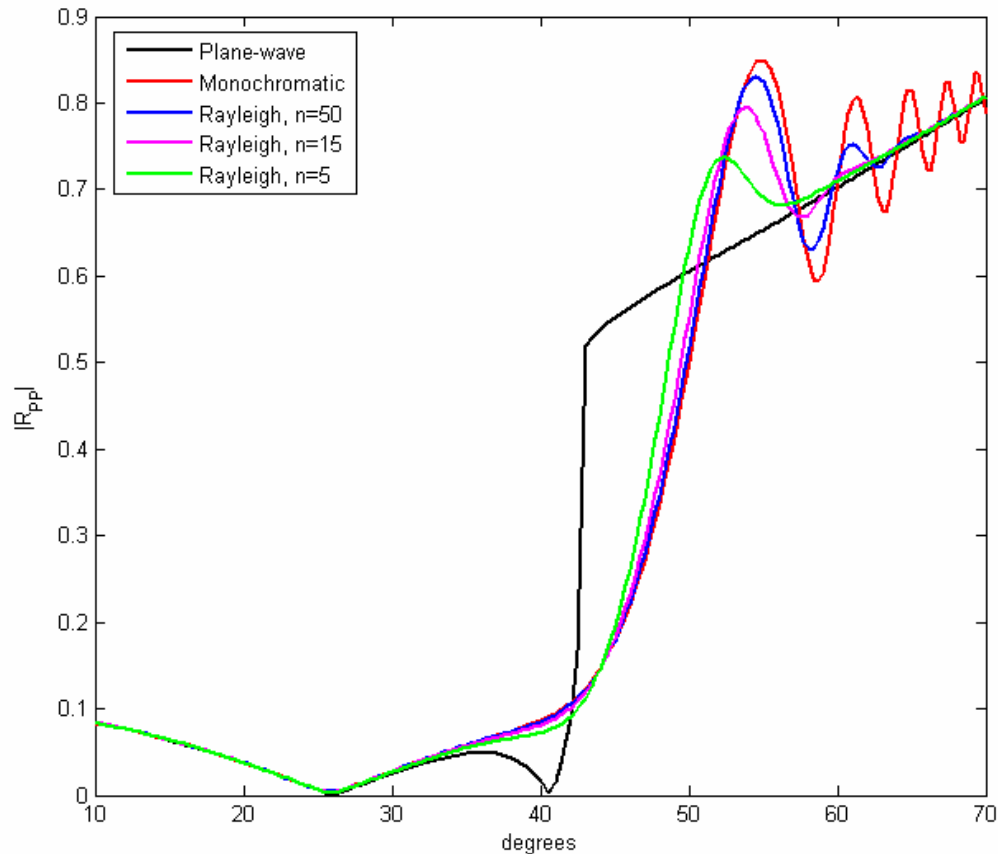

FIG. 7: The spherical-wave reflection coefficient curves for a series of Rayleigh wavelets, with the corresponding plane-wave curve and monochromatic spherical-wave curve. As *n* increases the Rayleigh curve behavior approaches that of the monochromatic curves.

SUMMARY AND COMMENTS

Spherical-wave reflection coefficient calculations have been re-expressed in terms of a weighting function. This weighting function depends explicitly on only three variables: angle of incidence, an integration variable, and a sphericity parameter. The latter subsumes frequency, overburden velocity and depth. The weighting function is analytic and may be readily programmed in terms of these three variables. A straightforward 1-D numerical integration then yields the normalized reflection coefficient.

Calculations with the method have shown that weighting functions for monochromatic wavelets are non-decaying and highly oscillatory. Comparing them to a series of weighting functions and reflection coefficient curves for increasingly narrow Rayleigh wavelets suggests that the less smooth the wavelet spectrum is, the more oscillatory the weighting function will be, and this will result in oscillations in the reflection coefficient curve as well. This suggests that the Ormsby wavelet would have an oscillatory weighting function as a result of slope discontinuities in its spectrum. Another report in this volume explores aspects of that question (Ursenbach and Haase, 2006).

Monochromatic spherical-wave reflection coefficients are a quantity of fundamental theoretical interest That they may also be of practical interest in interpreting monochromatic seismic surveys is discussed in another report in this volume (Ursenbach et al., 2006b).

ACKNOWLEDGEMENTS

REFERENCES

Aki, K., and P. G. Richards, 1980, Quantitative Seimology, vol. 1: W. H. Freeman.

Bortfeld, R., 1962, Reflection and refraction of spherical compressional waves at arbitrary plane interfaces: Geophysical Prospecting, **10**, 517-538.

Cagnaird, L., 1939, Réflexion et réfraction des ondes seismiques progressives: Gauthier-Villars.

Haase, A. B., 2004, Spherical wave AVO modeling of converted waves in elastic isotropic media: 2004 CSEG National Convention.

Hubral, P., and Tygel, M., 1985, Transient response from a planar acoustic interface by a new point-source decomposition in to plane waves: Geophysics, **50**, 766-774.

Hubral, P., and Tygel, M., 1989, Analysis of the Rayleigh pulse (short note): Geophysics, **54**, 654-658.

Krail, P. M., and H. Brysk, 1983, Reflection of spherical seismic waves in elastic layered media: Geophysics, **48**, 655-664.

Lamb, H., 1904, On the propagation of tremors over the surface of an elastic solid: Phil. Trans. Roy. Soc. (London) A, **203**, 1-42.

Macdonald, C., P. M. Davis, and D. D. Jackson, 1987, Inversion fo reflection traveltimes and amplitudes: Geophysics, **52**, 606-617.

Sommerfeld, A., 1909, Über die Ausbreitung der Wellen in der drahtlosen Telegraphie: Ann. Physik, **28**, 665-736.

Tygel, M., and P. Hubral, 1984, Transient representation of the Sommerfeld-Weyl integral with application to the point source response from a planar acoustic interface: Geophysics, **49**, 1495-1505.

Ursenbach, C. P., and A. B. Haase, 2004, An efficient method for calculating spherical-wave reflection coefficients: CREWES Research Report, **16**.

Ursenbach, C. P., and A. B. Haase, 2006, AVO modeling with non-zero phase spherical waves: CREWES Research Report, **18**.

Ursenbach, C. P., A. B. Haase, and J. E. Downton, 2006a, Improved modeling of spherical-wave AVO: CREWES Research Report, **18**.

Ursenbach, C. P., J. C. Bancroft, M. Bertram, H. Bland, A. B. Haase, D. C. Lawton, G. F. Margrave, and R. R. Stewart, 2006b, Proposal for polychromatic seismic survey: CREWES Research Report, **18**.